Flexure Pivot Oscillator With Intrinsically Tuned Isochronism

E. Thalmann[1]
École Polytechnique Fédérale de Lausanne (EPFL),
Instant-Lab,
Microcity, Rue de la Maladière 71b,
CH-2000 Neuchâtel, Switzerland
e-mail: etienne.thalmann@epfl.ch

M. H. Kahrobaiyan
École Polytechnique Fédérale de Lausanne (EPFL),
Instant-Lab,
Microcity, Rue de la Maladière 71b,
CH-2000 Neuchâtel, Switzerland
e-mail: mohammad.kahrobaiyan@epfl.ch

I. Vardi
École Polytechnique Fédérale de Lausanne (EPFL),
Instant-Lab,
Microcity, Rue de la Maladière 71b,
CH-2000 Neuchâtel, Switzerland
e-mail: ilan.vardi@epfl.ch

S. Henein
École Polytechnique Fédérale de Lausanne (EPFL),
Instant-Lab,
Microcity, Rue de la Maladière 71b,
CH-2000 Neuchâtel, Switzerland
e-mail: simon.henein@epfl.ch

The most important property for accurate mechanical time bases is isochronism: the independence of period from oscillation amplitude. This paper develops a new concept in isochronism adjustment for flexure-based watch oscillators. Flexure pivot oscillators, which would advantageously replace the traditional balance wheel-spiral spring oscillator used in mechanical watches due to their significantly lower friction, exhibit nonlinear elastic properties that introduce an isochronism defect. Rather than minimizing this defect, we are interested in controlling it to compensate for external defects such as the one introduced by escapements. We show that this can be done by deriving a formula that expresses the change of frequency of the oscillator with amplitude, i.e., isochronism defect, caused by elastic nonlinearity. To adjust the isochronism, we present a new method that takes advantage of the second-order parasitic motion of flexures and embody it in a new architecture we call the co-RCC flexure pivot oscillator. In this realization, the isochronism defect of the oscillator is controlled by adjusting the stiffness of parallel flexures before fabrication through their length L_p, *which has no effect on any other crucial property, including nominal frequency. We show that this method is also compatible with post-fabrication tuning by laser ablation. The advantage of our design is that isochronism tuning is an intrinsic part of the oscillator, whereas previous isochronism correctors were mechanisms added to the oscillator. The results of our previous research are also implemented in this mechanism to achieve gravity insensitivity, which is an essential property for mechanical watch time bases. We derive analytical models for the isochronism and gravity sensitivity of the oscillator and validate them by finite element simulation. We give an example of dimensioning this oscillator to reach typical practical watch specifications and show that we can tune the isochronism defect with a resolution of 1 s/day within an operating range of 10% of amplitude. We present a mock-up of the oscillator serving as a preliminary proof-of-concept.* [DOI: 10.1115/1.4045388]

Keywords: compliant mechanisms, design of innovative devices design of machine elements, mechanical oscillators, isochronism

1 Introduction

1.1 Limitations of Traditional Mechanical Watches. The time base used in classical mechanical watches is a harmonic oscillator consisting of a spiral spring attached to a balance wheel having a rigid pivot rotating on jeweled bearings. It has essentially the same architecture as when it was introduced by Huygens in 1675 [1], see Fig. 1. Subsequently, significant improvements were achieved in chronometric accuracy but seemed to have reached a plateau. The general consensus in horology is that the quality factor of the oscillator, a dimensionless number that characterizes the damping of an oscillator, needs to be improved for the accuracy to increase [2–4]. This phenomenon, first noted by Bateman [2], is not totally understood but is backed up by the apparent correlation between quality factor and timekeeping accuracy highlighted in Refs. [2–4], see Fig. 2. Despite concerted efforts by the watchmaking industry, the quality factor of classical balance spring oscillators barely surpasses 200, the friction in the bearing being the most important limitation to its quality factor [5]. According to Bateman's observation, a significant improvement in accuracy, i.e., better than 1 s/day error, would involve increasing the quality factor by an order of magnitude, as illustrated in Fig. 2 and as discussed in Refs. [2–4].

1.2 The Advent of Flexure-Based Watch Oscillators. A defining moment in watchmaking was the recent adoption by this very traditional industry of high-technology materials and techniques [6]—there are now mechanical watches having silicon components made using deep reactive ion etching (DRIE), for example, Ref. [7]. This acceptance paved the way for flexure-based watch oscillators for two reasons: replacing bearings by flexure pivots increases quality factor [5] and the minimal internal friction of monocrystalline silicon, by definition, increases quality factor, typically by an order of magnitude as compared with the classical metals used in watchmaking. For the reasons outlined in Sec. 1.1, flexure-based oscillators manufactured in silicon appear to be the breakthrough needed to achieve a new level in mechanical watch accuracy.

The watch industry has therefore taken on this challenge, and a number of prototypes and mechanical watches featuring flexure-based watch oscillators have recently been presented. The first of

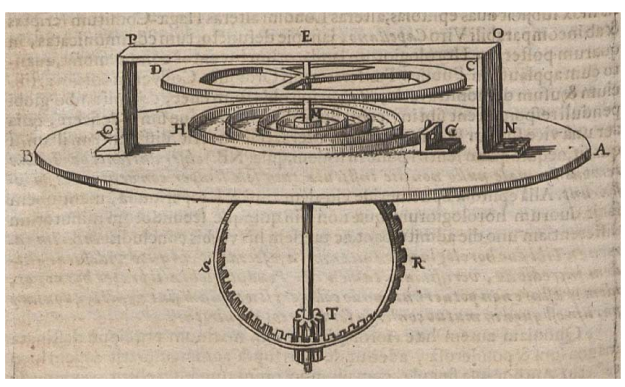

Fig. 1 Balance wheel-spiral spring oscillator drawn by Huygens in Ref. [1]

[1]Corresponding author.

Contributed by the Design Innovation and Devices of ASME for publication in the Journal of Mechanical Design. Manuscript received May 3, 2019; final manuscript received August 26, 2019; published online November 5, 2019. Assoc. Editor: David Myszka.

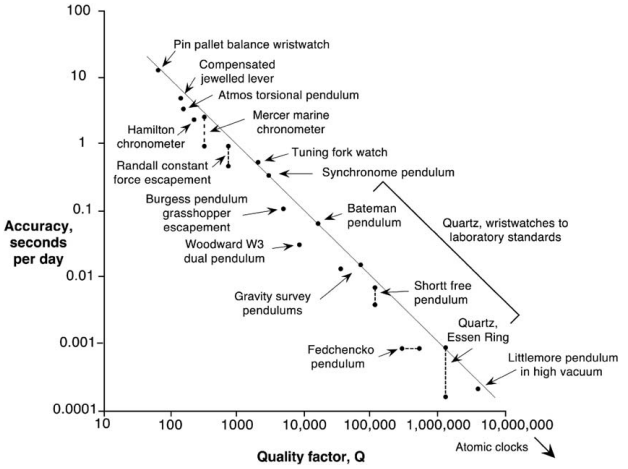

Fig. 2 Correlation between accuracy and quality factor [4]

these was the Genequand System discussed in Sec. 2.2 and presented in 2014 [8]. This mechanism already validated some expectations of flexure-based oscillators as it increased the quality factor and watch autonomy by an order of magnitude. More recent prototypes of flexure pivot oscillator were released in watches in 2017 [9,10] and 2019 [11,12]. These systems will however not be commented due to the lack of available information.

1.3 Advantages of Flexures. Apart from an increase in quality factor, the introduction of flexures brings additional advantages such as suppressing the need for lubrication, a traditional concern in watchmaking,[2] and simplifying assembly through monolithic fabrication [13,14].

Besides their bearing function, flexures have an intrinsic elastic restoring torque allowing them to conveniently replace the spring of the traditional oscillator. However, this restoring torque has nonlinear properties that introduce an isochronism defect, see Sec. 1.4, to which we present a solution.

1.4 Isochronism. Accurate timekeeping is essentially equivalent to having an oscillator with a period that is as regular as possible. Among the factors affecting the period are amplitude, orientation of gravity, and temperature. The most important of these factors is amplitude, and the independence of period from amplitude is called *isochronism*. This key element of precise timekeeping was first identified by Galileo who remarked that the pendulum would be a good time base since its period was independent of the oscillation amplitude. However, Mersenne and Descartes noted in 1636 that this was not accurate as they observed that the period of the pendulum slightly increases with amplitude [15]. Huygens then analyzed the problem mathematically and devised in 1656 a theoretically isochronous pendulum by replacing the rod with a flexible cord which unwinds off a cycloid [16], as depicted in Fig. 3. More details are given in Sec. 2.

In the case of a rotational oscillator consisting of a spring coupled to an inertial mass (such as the ones used in classical mechanical watches), the condition for isochronism is that the spring restoring torque must follow Hooke's law, i.e., be a linear function of the angular displacement. This condition complicates the use of flexures as oscillator springs since they exhibit nonlinear elastic properties. Different solutions already exist in order to achieve isochronism with flexure pivots but they all suffer from some limitation, see Sec. 2. There also exist other designs of flexure pivot oscillators which do not discuss isochronism [17].

[2]Watchmaking lore attributes a famous but most likely apocryphal quote to Abraham-Louis Breguet (1747–1823), one of the greatest watchmakers in history. When King Louis XVI asked him to make the perfect watch, he replied: "Give me the perfect oil and I will make you a perfect watch."

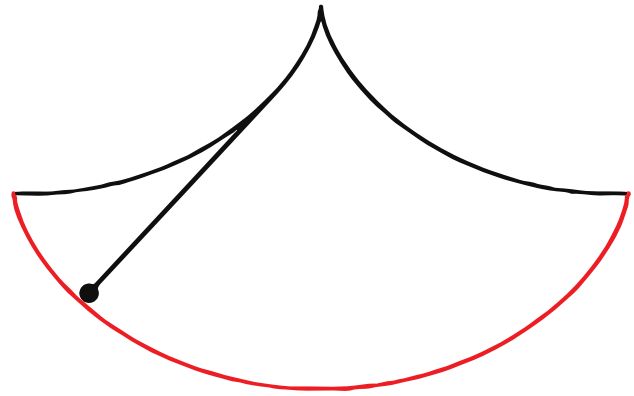

Fig. 3 Huygens' isochronism corrector for the pendulum using cycloidal cheeks

For the reasons outlined in Secs. 1.1–1.4, minimizing the isochronism defect of flexure-based mechanical watch oscillators is one of the most important issues to be addressed in order to significantly improve the chronometric accuracy of mechanical watches.

1.5 Gravity Sensitivity. The second crucial property for mechanical watch time bases is gravity insensitivity, which is the independence of oscillator frequency from its orientation with respect to gravity. In the case of flexure pivots, changes in the loading of the flexures can cause their stiffness to vary and consequently alter the frequency of the time base. Following our previous research in Ref. [18], we consider a flexure to be *gravity-insensitive* when there is no first-order effect of the load on its stiffness (assuming small loads).

1.6 Statement of Results. We design a new flexure pivot architecture that takes advantage of the parasitic shift of flexures, which is of the same order as the isochronism defect, to tune the isochronism of the oscillator without altering any other property crucial to its function such as nominal stiffness, operating stroke, gravity sensitivity, and center of rotation shift. This idea is new and is the principal contribution of the paper. The new architecture is called *co-RCC* flexure pivot oscillator and is depicted in Figs. 4 and 5.

We derive a formula that expresses the frequency of an oscillator in terms of the amplitude, thus characterizing the isochronism defect. We show that the variation from the nominal frequency with

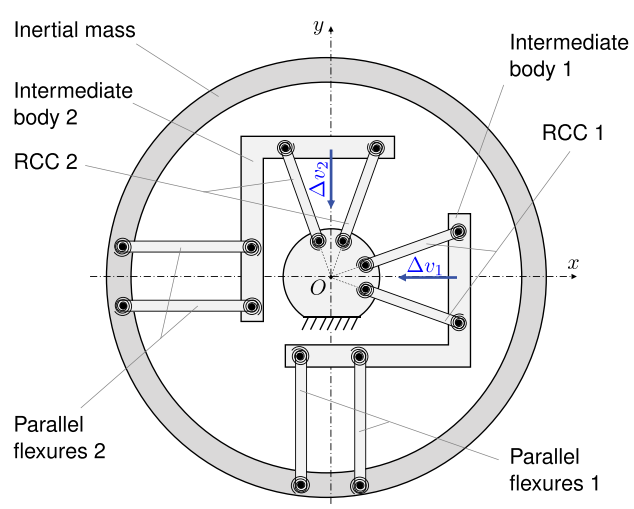

Fig. 4 Pseudo-rigid-body model of the co-RCC flexure pivot oscillator

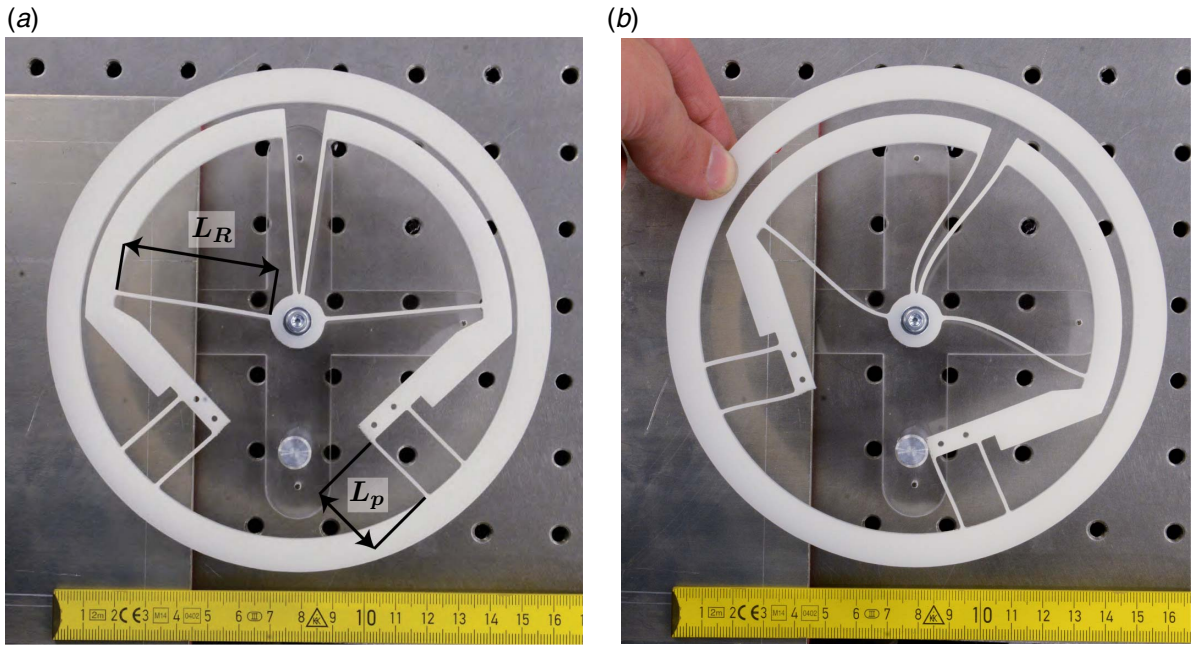

Fig. 5 Mock-up of the co-RCC flexure pivot oscillator (*a*) at rest position and (*b*) rotated by 26 deg, manufactured by laser cutting in polyoxymethylene to demonstrate the qualitative behavior of the pivot. Thickness: 5 mm, outer diameter: 150 mm, admissible angular stroke: ±26 deg. The length L_p is used to tune isochronism. To make our results independent of scale, we quantify this using the dimensionless parameter $\lambda = L_p/L_R$ (with L_R constant). In the rotated position *(b)*, an increased gap between the inertial mass and the intermediate bodies and a deformation of the parallel flexures can be observed as a result of the parasitic shift of the RCC pivots (Δv_1 and Δv_2 in Fig. 4).

amplitude depends on the restoring torque nonlinearity k_2 of the pivot and we focus our research on the study of this parameter, see Eq. (5). Rather than minimizing the isochronism defect by minimizing k_2, we are interested in controlling it to compensate for external defects such as the one introduced by escapements, see Sec. 2.2.

In the co-RCC design, the parasitic shift of the RCC flexures (labeled Δv_1 and Δv_2 in Fig. 4) deforms the neighboring parallel flexures, resulting in a contribution of the third-order of their stiffness to the restoring torque of the system. The nonlinearity k_2 (and thus the isochronism defect) of the system can thus be tuned, without affecting any other crucial property, by changing the stiffness of the parallel flexures, in particular by changing their length L_p, see Fig. 5(*a*). As opposed to the goal of Huygens' cycloidal cheeks that theoretically eliminate isochronism defect, our method is similar to modifying Hugyens' cycloidal cheeks to obtain any specific isochronism defect in a range around isochronism, i.e., around zero defect.

We call our method *intrinsic isochronism tuning* in opposition to the isochronism correctors previously realized through external mechanisms, see Sec. 2. We believe that our method is more adapted to modern manufacturing techniques and compact architectures.

We demonstrate in Sec. 6 that we are able to dimension a physical embodiment of the co-RCC oscillator that satisfies practical mechanical watch specifications, in particular a planar architecture that is compatible with current microfabrication processes and an isochronism tuning with a resolution of 1 s/day for a 10% amplitude variation from 15 deg nominal amplitude. We show that we can compensate for a realistic range of isochronism defects from −200 s/day to 400 s/day, see Fig. 6, and that we can achieve the specified isochronism defect tuning of order 1 s/day by varying the parallel flexure length L_p on the order 2.5 μm, see Sec. 6.2.1. In the co-RCC design, this tuning is implemented before manufacturing and is well within the range of current microfabrication techniques such as DRIE. Moreover, methods exist to adjust defects after manufacturing, in particular removing microns of matter by laser ablation in order to lengthen L_p, see Fig. 5(*a*). This technique is being used in the completely automated adjustment of the daily rate of mechanical watches [19].

Figure 6 displays the *daily rate*, that is, the gain or loss of the timekeeper in seconds per day with respect to a reference frequency, see Eq. (7), of a co-RCC oscillator for different values of the parallel flexure length L_p, as quantified by the dimensionless parameter $\lambda = L_p/L_R$, see Fig. 5(*a*). The parameter α, which describes the angle between the RCC flexures, see Sec. 4.2, also affects the isochronism but is not used for fine-tuning as it also affects the gravity sensitivity of the oscillator. Details are provided in Secs. 4 and 6.2.

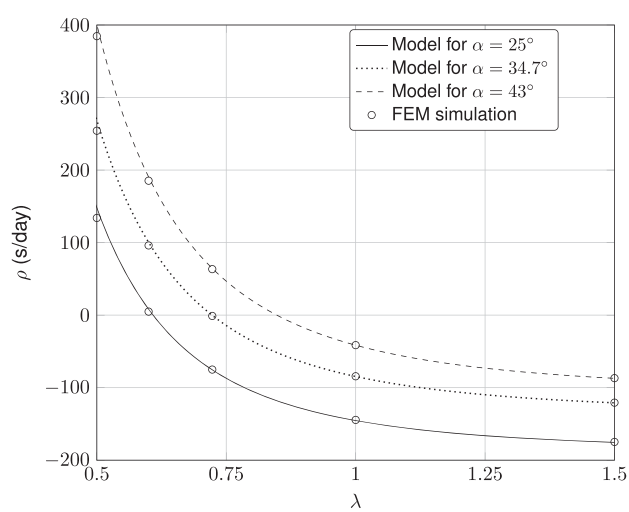

Fig. 6 Daily rate ρ versus λ of a co-RCC at $\Theta = 16.5$ deg with respect to the reference amplitude $\Theta_1 = 15$ deg. The dimensions of the oscillator are given in Sec. 6.2. The results obtained with the analytical model with $\alpha = 25$, 34.7, and 43 deg are compared with those obtained by the FEM simulation.

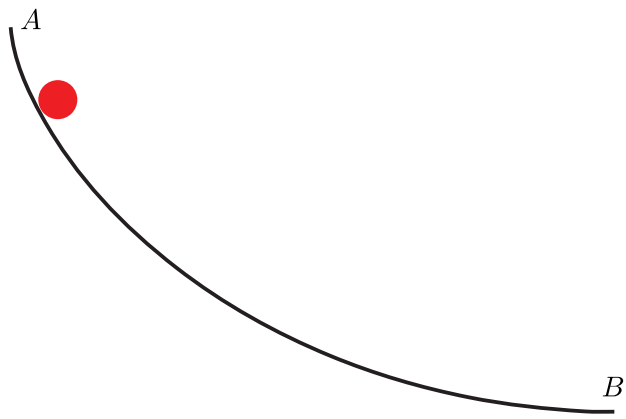

Fig. 7 Ball sliding along a cycloid

The architecture is also gravity-insensitive, thus achieving two of the conditions for accurate timekeeping. The design principle used to achieve gravity insensitivity is similar to the *co-differential* concept that we introduced in Ref. [18]. The two concepts are compared in Sec. 3.4.1.

The analytical models derived for the isochronism and gravity sensitivity of the co-RCC, respectively, in Secs. 4 and 5, are validated by numerical simulation in Sec. 6.3.

In order to be used in a watch, this oscillator needs an escapement. However, this topic is not considered in this article except for specifying a nominal amplitude of operation of 15 deg, under the assumption that this amplitude is sufficient for an escapement to work, see Sec. 6.1. The third condition for accurate timekeeping, insensitivity to temperature, is beyond the scope of this article. We assume that it can be achieved through already established temperature-invariant materials, such as the ones described in Refs. [7,20,21] or temperature compensation techniques.

2 State of the Art

2.1 Isochronism Correction for the Pendulum. In 1656, Huygens confirmed mathematically Mersenne and Descartes' observation that the pendulum was not isochronous and devised an isochronous pendulum in three stages [22]. First, he sought the curve from A to B shown in Fig. 7 down which an object will slide from rest without friction under gravity to point B in the same time, irrespective of its starting point between A and B. He showed that this so-called *tautochrone curve* is a cycloid.[3] Second, he introduced the notion of involute, the curve traced by the end of a string wrapping around another curve (the evolute). Third, he showed that the involute of a cycloid is another cycloid. The result is a pendulum consisting of a suspension thread that wraps around cycloidal cheeks and a bob that consequently follows the tautochrone curve, see Fig. 8. This idea was implemented in a clock in 1657, see Fig. 9. Note that another way to look at the effect of the cycloidal cheeks is that they change the effective length of the pendulum as it swings, thus altering its frequency. This solution is theoretically correct but does not appear to work well in practice, as explained in Refs. [24,25]. It was quickly abandoned in favor of rigid rods with small amplitudes. It should be noted that the small-amplitude solution was not considered by Huygens since he was interested in marine chronometers, which necessitated large amplitudes. Subsequently, there was much research on pendulum suspensions and isochronism [3,25,26]. We are currently studying the possibility of applying the results of this paper to this subject.

[3]41 years later, Johann Bernoulli proved that this was also the *brachistochrone*, i.e., the curve of fastest descent under gravity between two points [23].

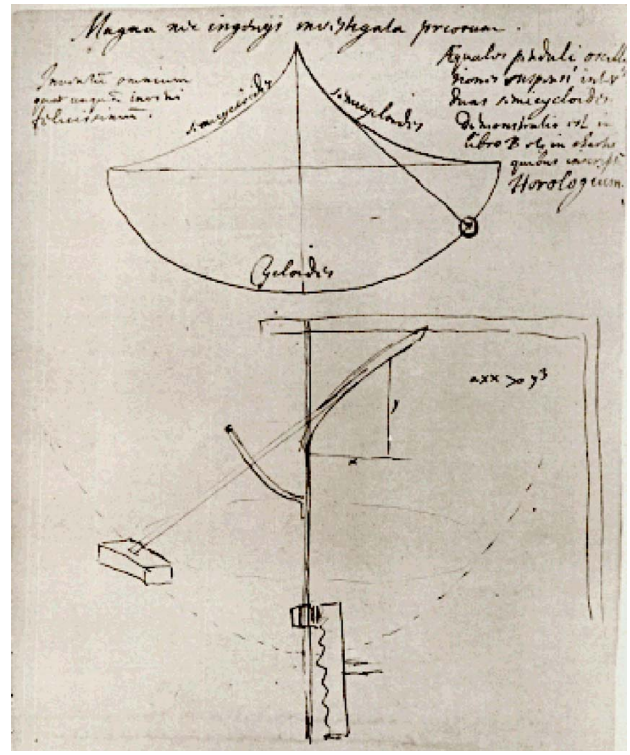

Fig. 8 Huygens' drawing of the isochronous pendulum [27, note to letter from Ch. Huygens to H. Oldenburg, June 24, 1673]

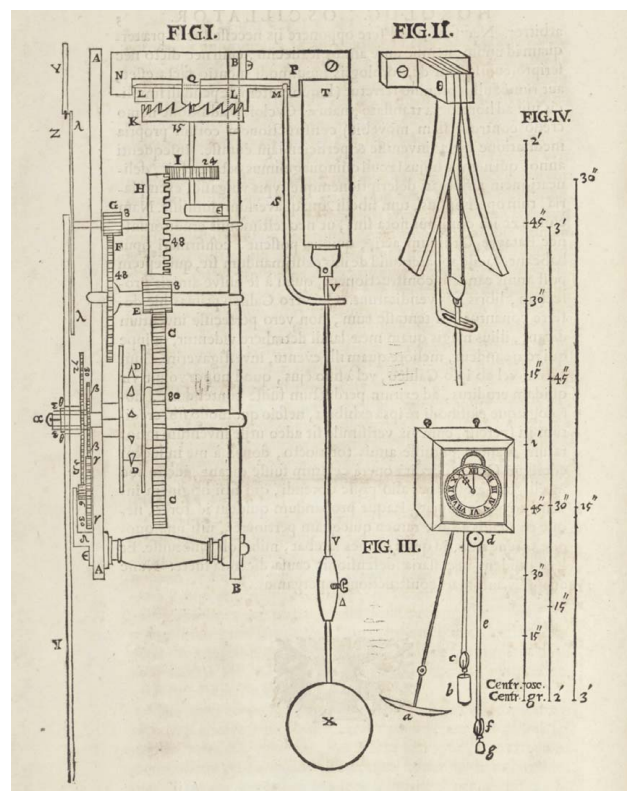

Fig. 9 Huygens' clock design with cycloidal cheeks shown in Fig. II [16]

2.2 Flexure Pivot Oscillator Isochronism Correction. The first flexure pivot oscillator for a mechanical watch was introduced in the 2014 Genequand system [8]. The basis of the Genequand system was a flexure-based escapement, similar to the grasshopper

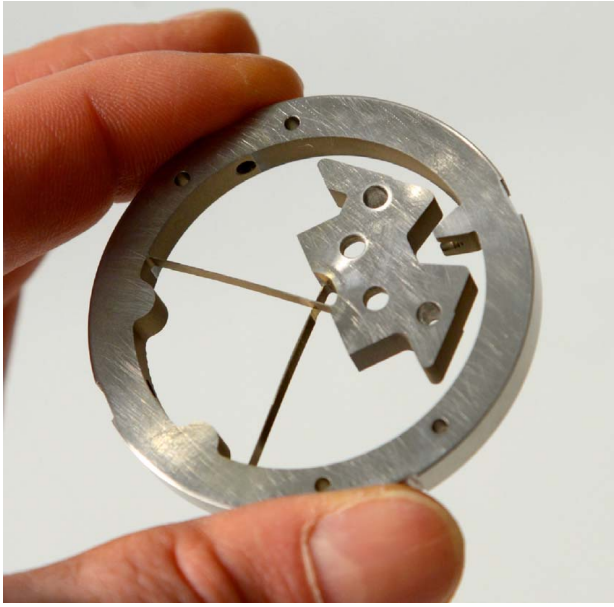

Fig. 10 Crossed flexure pivot with crossing point minimizing its gravity sensitivity [31]

escapement invented by Harrison around 1722 [28]. The crossed flexure pivot, introduced by Wittrick [29] and depicted in Fig. 10, was added at a later stage in order to implement the system at the watch scale. The oscillator is gravity-insensitive thanks to a particular value of the crossing point of its flexures [30,31] but has an isochronism defect. A system was developed by Henein and Schwab [32] to address this defect as well as the one caused by the escapement. It is indeed known that escapements introduce isochronism defects and this property has already been used in clocks to compensate for the intrinsic defect of pendulums [24,33]. This is also why, in this article, we are interested in controlling the defect of the oscillator rather than minimizing it.

2.2.1 The Genequand System Isochronism Corrector. The isochronism corrector developed for the Genequand system [32] uses flexible blades that come in contact with the escapement anchor for part of the stroke, introducing a discrete change in stiffness. Since the anchor is always in contact with the oscillator, the change directly affects the oscillator. Figure 11 shows the contact between pin 9 of the anchor and flexure 14. Due to the mechanical stop 22, the contact happens only when the pin is to the right of axis *A*. The discrete stiffness variation always happens at the same angular position, such that the ratio of time that the oscillator spends with one stiffness to the time spent with the other stiffness depends on the amplitude of oscillation. This introduces a variation of frequency with an amplitude that can be used to correct the isochronism. The mechanism relies on three setting inputs and is complex to tune. It also introduces shocks at the contact point 14a that can have undesired consequences.

2.2.2 Isochronous Crossed Flexure Pivots. We explained in Secs. 1.4 and 1.5 that the crucial properties for a mechanical watch timebase are isochronism and gravity insensitivity. In Ref. [18], we presented a pivot capable of reaching both goals since the crossing point of its flexures can be used to set the isochronism defect and its architecture is intrinsically gravity-insensitive.

The crossed flexure pivot of the Genequand system used a special value of the crossing point of its flexures to reach gravity insensitivity and this parameter could thus not be used to set its isochronism defect. Di Domenico et al. [34] solved this issue by using the angle α between the flexures in addition to their crossing point to set the isochronism defect while minimizing gravity sensitivity, as depicted in Fig. 12(*a*).

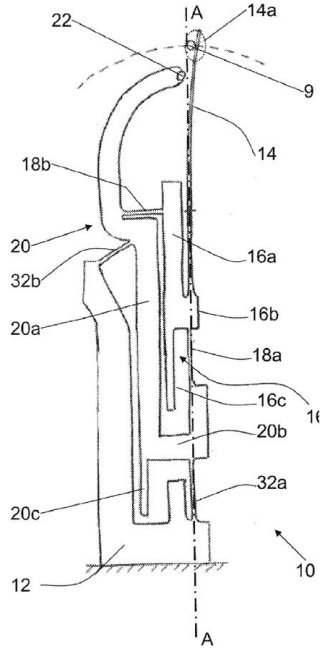

Fig. 11 Figure from the Genequand system isochronism corrector patent [32]

These methods do not qualify as isochronism tuning according to our definition in Sec. 1.6: changing the crossing point or the angle between the flexure also affects the gravity sensitivity and center shift of the pivot [35,36]. The architecture illustrated in Fig. 12(*b*), where two crossed-flexure pivots are mounted head-to-tail [37], seems to eliminate the gravity-sensitivity and center shift issues through its symmetry, allowing for isochronism tuning using the angle α. It is indeed known that α has no significant impact on the nominal stiffness and stroke of the oscillator [38]. This architecture however has a redundant degree-of-freedom (DOF): the intermediate body 20 can rotate without moving the inertial body 201. Such a redundant DOF can be excited by external forces and affect the stroke of the pivot or start vibrating [13], thus disturbing the oscillator.

3 Design and Kinematics of the Co-RCC Flexure Pivot

3.1 The Concept. The design principle behind the co-RCC is that two *remote center of compliance* flexure pivots (RCC pivots) [13] "collaborate" to form a pivot with superior properties: the parasitic center shift of the RCC pivots is used to tune the restoring torque nonlinearity of the co-RCC and the effect of the parasitic shift on the inertial body is significantly reduced. Additionally, external loads on the main rigid body are shared between the two RCC pivots in a way that makes the co-RCC gravity-insensitive. Its architecture is depicted in Fig. 4, where the flexures are represented by their pseudo-rigid-body equivalent [14]. The rigid bars with pin joints and rotational springs at their extremities have equivalent force-deflection characteristics to the leaf springs used in the physical embodiment in Fig. 5.

We explain the design of the co-RCC by decomposing it into subelements. We start with the RCC pivot in Sec. 3.2, then add a slider to it to form the half co-RCC in Sec. 3.3, and finally combine two of these elements in parallel to form the co-RCC in Sec. 3.4.

3.2 The RCC Flexure Pivot. The RCC pivot, sometimes also referred to as *isosceles-trapezoidal flexural pivot* [36], is illustrated in Fig. 13. It is a particular case of the crossed flexure pivot [29] where the flexures cross symmetrically outside of their physical structure. The intersection of the flexures defines (to a first

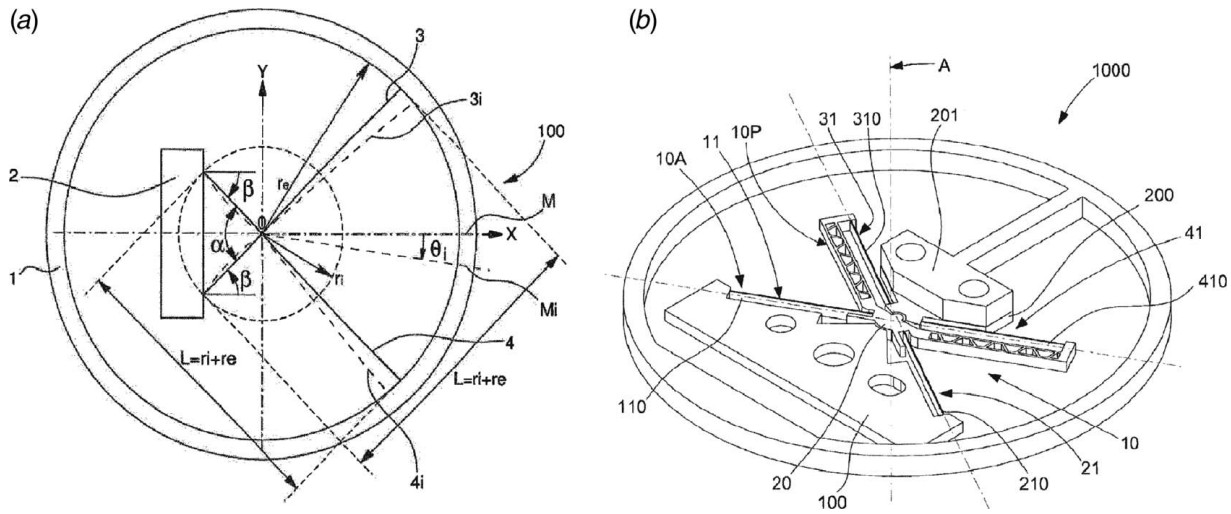

Fig. 12 Crossed flexure pivot oscillators from (*a*) Ref. [34] and (*b*) Ref. [37], whose angle α between the flexures is used to minimize the isochronism defect

approximation) the axis of rotation of the pivot [39], see axis w in Fig. 13. This pivot has been chosen due to its advantageous planar architecture and negative restoring torque nonlinearity that will be used to tune the isochronism, see Sec. 4.3.

We define a local coordinate system for the RCC pivot whose origin lies at the intersection of the neutral axes of the flexure beams as depicted in Fig. 13. Axis v is parallel to the bisector of the angle formed by the flexures, axis w is perpendicular to the plane holding the neutral axes, and u is the third orthogonal axis.

3.2.1 Parasitic Center Shift. The center of rotation of the RCC pivots exhibits a so-called parasitic shift. Zhao and Bi [35] give analytical expressions for the components of the parasitic shift along the u and v axes of the RCC local coordinate system, see Fig. 13. For slender flexures[4] and small rotations, the v-component is of second-order of the rotation angle and the u-component, which is of third-order, can be neglected.

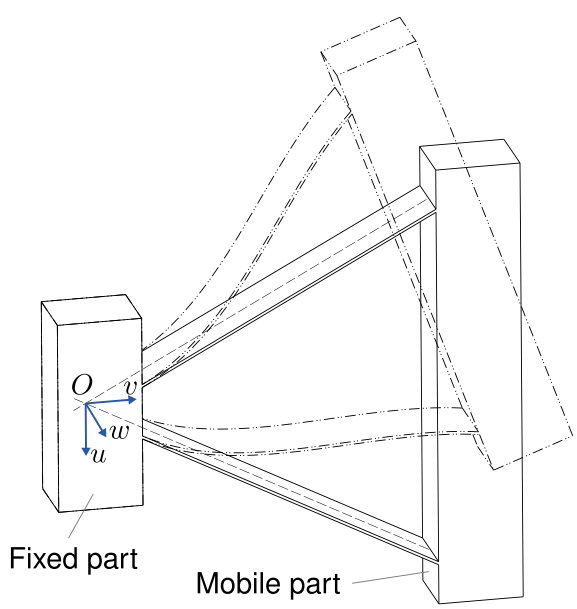

Fig. 13 Remote center of compliance (RCC) flexure pivot in undeflected position (solid lines) and rotated about the *w*-axis (dashed lines)

3.3 The Half Co-RCC. The half co-RCC element depicted in Fig. 14 is obtained by adding a slider between the RCC and the main rigid body, where the axis of the slider is parallel to the v-axis of the RCC. This element has two degrees-of-freedom: one rotation around center O and one translation along v. As we will see in Sec. 3.4, the additional DOF allows to tune the isochronism of the oscillator, to achieve gravity insensitivity and to avoid over-constraining[5] the co-RCC.

3.4 The Co-RCC Flexure Pivot. The co-RCC depicted in Fig. 15 consists of two half co-RCC arranged in parallel, at a 90 deg angle, with coinciding axes of rotation. The first half co-RCC consists of the "RCC 1" in series with the "Slider 1" and the second consists of the "RCC 2" in series with the "Slider 2." They share the same main rigid body, and the center of mass of the system is placed at its center of rotation O. We assume that the intermediate bodies have negligible mass. The system has one DOF and no overconstraint in the xy-plane. Note that the out-of-plane overconstraints can be overlooked assuming that the mechanism is monolithically fabricated. Taking advantage of the elasticity of the RCC flexures, if the main rigid body has a non-zero inertia J, this flexure pivot behaves as a rotational oscillator.

Through the parallel arrangement of two half co-RCC elements, the translation of the main rigid body allowed by one-half co-RCC is blocked by the other one. As a result, when the system rotates, the parasitic shift of the RCC pivots, which is along the sliding axis of their respective half co-RCC (see Sec. 3.2.1), does not affect the main rigid body (as this motion is blocked by the other half co-RCC). The motion of the main rigid body closely approximates a rotation about point O, which we define as the rotation of the co-RCC.

It follows that the parasitic shifts of each RCC pivot results in a relative linear motion, labeled Δv_1 or Δv_2 in Fig. 15, between the intermediate body to which it is attached and the main body. In the flexure implementation of Fig. 5, the sliders are realized with parallel flexures which are known to closely approximate a

[4]We consider a flexure to be slender if, in the uv-plane of Fig. 13, length > 10 × thickness. This is the case in our analysis.

[5]A mechanism is overconstrained when its mobility obtained through Grübler's formula [40] is less than its actual DOF. This can lead to important and unpredictable variations of the stiffness of flexure mechanisms and the stresses in their flexures [13].

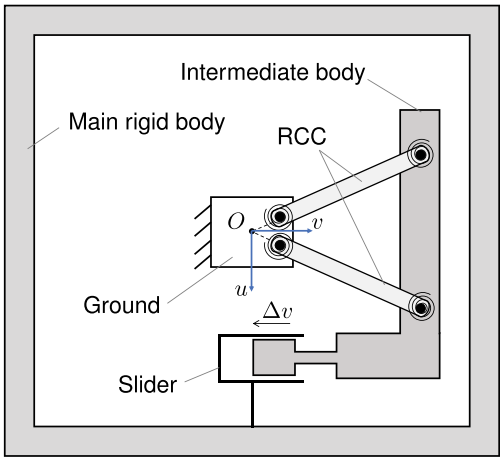

Fig. 14 Design of the half co-RCC

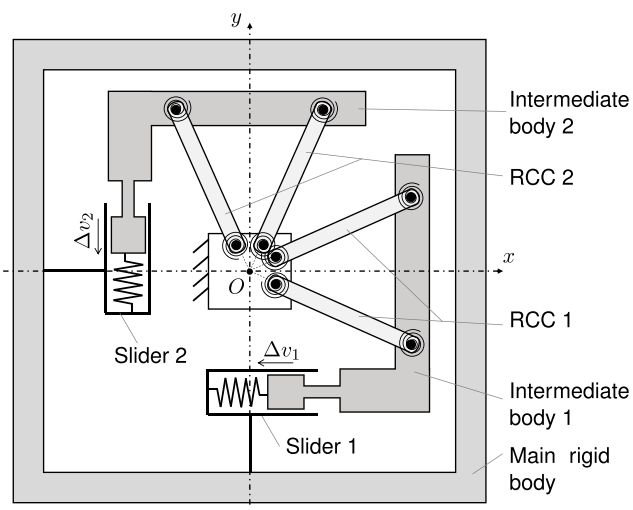

Fig. 15 Design of the co-RCC flexure pivot

sliding motion[6] [13]. The deflection of these flexures caused by the RCC parasitic shift is of second-order of the rotation angle [35] and their stiffness, depicted as linear springs in Fig. 15, can be used to tune the isochronism of the oscillator, see Sec. 4.3.

We manufactured a mock-up to validate qualitatively the kinematics of the co-RCC pivot, see Fig. 5. This hardware showed that the system behaves qualitatively as a pivot (one DOF and a motion of the main body closely approximating a rotation about point O) while having a linear relative motion between the intermediate bodies and the main body, see Fig. 5(*b*).

Remark. The design can be generalized by using any type of crossed flexure pivot, by using rotational joints instead of slider joints, by changing the order of the joints of the half co-RCC and by using any type of flexures that have the force-deflection characteristics of the PRBM depicted in Fig. 4.

3.4.1 Gravity Sensitivity and Comparison With the Co-Differential. An additional advantageous property of the co-RCC architecture is that it follows the co-differential concept introduced in Ref. [18] to achieve gravity-insensitivity. In the co-differential concept, the flexures providing the rotational stiffness of the pivot are always loaded with equal but opposite forces, which minimizes the influence of an external load, such as gravity, on the overall stiffness. This effect is obtained by placing the flexures symmetrically at a 180 deg rotation.

In the co-RCC, the same compensating effect is obtained through the fact that the sliders do not transmit any load along their axis of motion (under the assumption that their stiffness is much lower than that of the "blocked" degrees-of-freedom). Thus, when an external load acts on the main rigid body, each half co-RCC element is loaded with the component of that force along its local u-axis and the RCC flexures are loaded with equal but opposite forces.

4 Analytical Model: Isochronism

In this section, we derive an analytical model for the isochronism defect of the co-RCC flexure pivot oscillator and show how it can be tuned by modifying only the non-linearity of the pivot's restoring torque. This effect is treated separately from the gravity sensitivity, itself treated in Sec. 5, by assuming no external load ($F = 0$).

Remark. The assumption to decouple both effects in the analysis is reasonable since the terms combining F and θ have order >2, see Eq. (27). They are thus negligible under our small load and small displacement assumptions.

4.1 Definition of Isochronism Defect. We first consider the ideal case of the simple rotational harmonic oscillator satisfying

$$J\ddot{\theta} + k\theta = 0 \tag{1}$$

where $\theta = \theta(t)$ is angular displacement, J is the moment of inertia, and k is the rotational stiffness. This has solution

$$\theta(t) = \Theta \sin(\omega_0 t + \Phi) \tag{2}$$

where Θ is the amplitude, $\omega_0 = \sqrt{k/J}$ is the angular frequency, and Φ is a phase depending on initial conditions.

In the ideal case, the angular frequency ω_0 is independent of the amplitude Θ, so there is isochronism. However, this is not true in practice and this, in fact, is the exact subject of this article. We therefore consider the perturbed harmonic oscillator

$$\theta(t) = \Theta \sin(\omega t + \Phi) \tag{3}$$

in which the angular frequency $\omega = \omega(\Theta)$ depends on the amplitude Θ.

We showed in Ref. [41] that, for a rotational oscillator with constant inertia J and nonlinear restoring torque, the angular frequency at small amplitude satisfies

$$\omega(\Theta) = \omega_0\left(1 + \frac{3\mu}{8}\Theta^2\right) \tag{4}$$

where μ is the relative nonlinearity of the restoring torque introduced in Ref. [18].

For a pivot whose restoring torque

$$M = k_0\,\theta + k_2\,\theta^3 + \mathcal{O}(\theta^5) \tag{5}$$

is expressed by a power series having only odd terms (since restoring torque is an odd function of the angle), we call k_2 the *nonlinearity* of the restoring torque and

$$\mu = \frac{k_2}{k_0} \tag{6}$$

the *relative nonlinearity* of the restoring torque. Note that, in this case, the nominal frequency of the oscillator is $\omega_0 = \sqrt{k_0/J}$.

Equation (4) gives an explicit expression for the isochronism defect; the subject of this paper will be the study of its tuning by modifying only the nonlinearity k_2.

In order to apply Eq. (4) to provide numerical isochronism data, we choose a *reference amplitude* Θ_1 with corresponding frequency

[6]The parallel flexures also exhibit a parasitic motion that is of second-order of the sliding motion [13]. In the co-RCC geometry, this motion is of fourth-order of the rotation angle and can thus be neglected.

ω_1. One then defines the *daily rate* [42] by

$$\rho = 86400 \frac{\omega - \omega_1}{\omega_1} \tag{7}$$

that is, the gain or loss of the timekeeper, in seconds per day, with respect to the reference frequency. Daily rate gives a precise measure of the (hopefully small) isochronism defect. Applying Eq. (4) gives the following explicit formula for the daily rate in terms of amplitude, the reference amplitude and μ

$$\rho = 32400\mu \frac{\Theta^2 - \Theta_1^2}{1 + 3\mu\Theta_1^2/8} \tag{8}$$

4.1.1 Alternate Definition of Isochronism Defect. In previous research, we adopted an alternate definition of isochronism defect that proved useful to the watchmaking industry [43]. *This definition will not be used in this paper*, but we derive Eq. (11) below so that our results can be easily translated into that notation.

As above, a reference amplitude Θ_1 is chosen with corresponding frequency ω_1, with daily rate ρ as above corresponding to a neighboring amplitude Θ. The *relative isochronism defect* is then defined by

$$\sigma = \frac{\rho}{\Theta_{\%}} \tag{9}$$

where

$$\Theta_{\%} = 100 \frac{\Theta - \Theta_1}{\Theta_1} \tag{10}$$

so that the isochronism defect is expressed as seconds per day in terms of relative amplitude variation, expressed in %. Note that this definition of isochronism defect is highly dependent on the choice of reference amplitude.

Substituting Eq. (4) into Eq. (9) yields the relative isochronism defect of an oscillator with relative nonlinearity μ

$$\sigma = \frac{324\mu\,\Theta_1(\Theta + \Theta_1)}{1 + 3\mu\,\Theta_1^2/8} \tag{11}$$

Remark. In Ref. [43], the relative isochronism defect was computed in terms of relative oscillator energy $E_{\%}$, not relative amplitude $\Theta_{\%}$, since it was not possible to identify the amplitude of the 2 degrees-of-freedom oscillators considered there. Since oscillator energy is proportional to the square of amplitude, it is easily shown that, under suitable conditions, the relative isochronism defects with respect to energy and with respect to amplitude differ by approximately a factor of 2.

4.2 Restoring Torque Nonlinearity of the Co-RCC. In Sec. 4.1, we showed the relationship between restoring torque nonlinearity and isochronism defect. We now derive an expression for the nonlinearity of the co-RCC, which we use to tune its isochronism defect. Our analysis is valid under the following assumptions:

- We consider the flexure element as springs and the other bodies as rigid. Figure 16 shows such model where the RCC pivots have a rotational stiffness k_{RCC1} and k_{RCC2} and the sliders have a translation stiffness k_{p1} and k_{p2}.
- The motion of the sliders (Δv_1 and Δv_2) corresponds to the parasitic motion of the RCC pivots along their local v-axis, see Sec. 3.4.
- The system is symmetric: $k_{RCC1} = k_{RCC2} = k_R$, $k_{p1} = k_{p2} = k_p$, and $\Delta v_1 = \Delta v_2 = \Delta v$.
- The rotations are small and we express terms using series expansions around $\theta = 0$.

We proceed with the following steps:

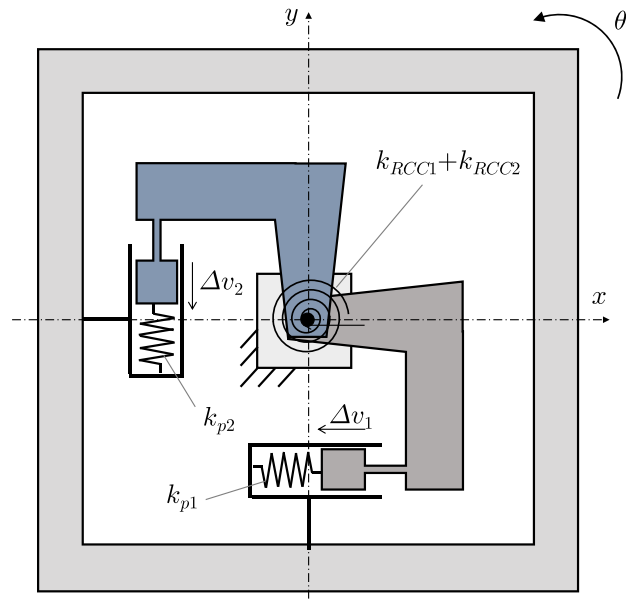

Fig. 16 Spring model of the co-RCC

(1) Express the restoring torque and motion of the spring elements for a given rotation of the co-RCC.
(2) Express the strain energy of the co-RCC for a given rotation.
(3) Derive the restoring torque of the co-RCC from its total strain energy.
(4) Express the restoring torque nonlinearity of the co-RCC.

4.2.1 Restoring Torque and Motion of the Spring Elements. The nonlinear restoring torque of the spring elements can be expressed by series expansion in the same way as Eq. (5), giving

$$M_R(\theta) = k_{R,0}\,\theta + k_{R,2}\,\theta^3 + \mathcal{O}(\theta^5) \tag{12}$$

for the RCC pivots and

$$M_p(\Delta v) = k_{p,0}\,\Delta v + k_{p,2}\,\Delta v^3 + \mathcal{O}(\Delta v^5) \tag{13}$$

for the parallel flexures.

The displacement of the parallel springs for a given rotation θ of the system corresponds to the parasitic motion of the RCC pivots along v given in Ref. [35]:

$$\Delta v = -\frac{(9\delta^2 + 9\delta + 1)L_R}{15\cos\alpha}\theta^2 + \mathcal{O}(\theta^4) \tag{14}$$

where L_R is the length of the RCC flexures, α is the half-angle between them, and $\delta = d/L_R$ describes their intersection point, see Fig. 17.

4.2.2 Strain Energy. The strain energy of the co-RCC for a rotation θ is the sum of the potential energies of each spring

$$U = 2\left(\int_0^{\theta} M_R(\nu)\,d\nu + \int_0^{\Delta v} M_p(\nu)\,d\nu\right) \tag{15}$$

which, when substituting with Eq. (12)–(14), yields

$$U = k_{R,0}\,\theta^2 + \left(\frac{1}{2}k_{R,2} + \frac{(9\delta^2 + 9\delta + 1)^2 L_R^2}{225\cos^2\alpha}k_{p,0}\right)\theta^4 + \mathcal{O}(\theta^6) \tag{16}$$

4.2.3 Restoring Torque. The restoring torque of the co-RCC for a rotation θ is the derivative of the strain energy U with

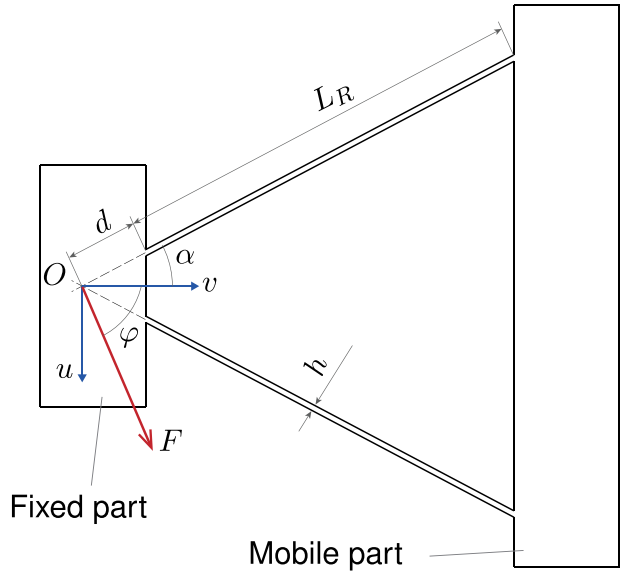

Fig. 17 Top view of an RCC flexure pivot with geometric parameters and a load acting at its center of rotation

respect to θ

$$M_c = \frac{dU}{d\theta} = 2k_{R,0}\,\theta + \left(2k_{R,2} + \frac{4(9\delta^2+9\delta+1)^2 L_R^2}{225\cos^2\alpha}k_{p,0}\right)\theta^3 + \mathcal{O}(\theta^5) \tag{17}$$

The nominal stiffness of the RCC pivot $k_{R,0}$ and parallel flexures $k_{p,0}$ can be substituted with the expressions from Ref. [13]

$$k_{R,0} = \frac{8EI_R(3\delta^2+3\delta+1)}{L_R} \quad \text{and} \quad k_{p,0} = \frac{24EI_p}{L_p^3} \tag{18}$$

where E is Young's modulus for the flexures, I_R and I_p are the area moment of inertia of the cross-section of the RCC and parallel flexures, respectively, and L_p is the length of the parallel flexures, see Fig. 5(*a*), yielding

$$M_c = \frac{16EI_R(3\delta^2+3\delta+1)}{L_R}\,\theta + \left(2k_{R,2} + \frac{32(9\delta^2+9\delta+1)^2 EI_p L_R^2}{75\cos^2\alpha L_p^3}\right)\theta^3 + \mathcal{O}(\theta^5) \tag{19}$$

4.2.4 Restoring Torque Nonlinearity. The nonlinearity of the co-RCC

$$k_{c,2} = 2k_{R,2} + \frac{32(9\delta^2+9\delta+1)^2 EI_p L_R^2}{75\cos^2\alpha L_p^3} \tag{20}$$

follows from Eq. (19) and its relative nonlinearity according to Eq. (6) is

$$\mu_c = \mu_R + \frac{2(9\delta^2+9\delta+1)^2}{75(3\delta^2+3\delta+1)\cos^2\alpha\lambda^3}\frac{I_p}{I_R} \tag{21}$$

where

$$\lambda = L_p/L_R \tag{22}$$

is the dimensionless ratio of the length of the parallel flexures to the length of the crossed flexures, see Fig. 5(*a*), and

$$\mu_R = \frac{k_{R,2}}{k_{R,0}} \tag{23}$$

is the relative nonlinearity of the RCC flexures. We showed in Ref. [17] that $k_{R,2}$ cannot be calculated accurately using Euler-Bernoulli beam theory and overcome this issue by calculating it numerically, see Sec. 6.3.

Remark. It is assumed here that Young's modulus is the same for all flexures. If an anisotropic material is chosen, the difference in Young's modulus should be taken into account in the calculation of the nonlinearity.

4.3 Isochronism Tuning. Our objective is to tune the isochronism defect of the co-RCC without affecting any other crucial property. Equation (4) shows that isochronism can be tuned through the restoring torque nonlinearity and Eq. (20) shows the parameters influencing it. Several parameters could be used to vary the isochronism defect but only those of the parallel flexures, L_p and I_p, will have no effect on the other crucial properties of the oscillator such as nominal stiffness (and consequently nominal frequency), gravity sensitivity, or stroke, which only depend on the geometry of the RCC flexures. The length L_p of the parallel flexures is a convenient parameter for the tuning whereas the range of I_p is limited by constraints on the flexure thickness h and height b (in the z-direction) imposed by manufacturing.

The isochronism tuning achieved by modifying L_p is expressed in terms of daily rate by substituting Eq. (21) into Eq. (8), yielding

$$\rho = \frac{32400\left(\mu_R + \frac{2(9\delta^2+9\delta+1)^2}{75(3\delta^2+3\delta+1)\cos^2\alpha}\frac{I_p}{I_R}\left(\frac{L_R}{L_p}\right)^3\right)(\Theta^2-\Theta_1^2)}{1+\frac{3}{8}\left(\mu_R + \frac{2(9\delta^2+9\delta+1)^2}{75(3\delta^2+3\delta+1)\cos^2\alpha}\frac{I_p}{I_R}\left(\frac{L_R}{L_p}\right)^3\right)\Theta_1^2} \tag{24}$$

In order to be able to set the sign of the isochronism defect, the RCC pivot is chosen to have a negative nonlinearity μ_R [41] such that the two terms forming the nonlinearity in Eq. (20) are of opposite sign. The sign of the defect then depends on the relative magnitude of these two terms. The tuning obtained with Eq. (24) is displayed in Fig. 6 where the dimensionless ratio $\lambda = L_p/L_R$ is used to make the results independent of scale.

5 Analytical Model: Gravity Sensitivity

As explained in Sec. 4, we treat the gravity sensitivity of the co-RCC flexure pivot oscillator separately from its isochronism. This is done by assuming a small amplitude, i.e., θ^2 negligible in this part of the analysis.

Our gravity sensitivity analysis follows the method introduced in Ref. [18] to express the change in stiffness of the oscillator caused

by gravity loading and to calculate the resulting timekeeping defect. The development consists of the steps below, following the structure of Sec. 3:

(1) Calculate the rotational stiffness of an RCC pivot subject to a force applied at point O.
(2) Calculate the rotational stiffness of a half co-RCC subject to a force applied at point O.
(3) Calculate the rotational stiffness of a co-RCC subject to a force applied at point O.
(4) Express the gravity sensitivity of the co-RCC in terms of daily rate.

The analysis is valid under the following assumptions:

- The loads are small and we express terms using series expansions around $F=0$.
- The rotations are small and we express terms using series expansions around $\theta=0$.
- The RCC flexures are not subject to shear or torsion and, with the previous assumption, Euler-Bernoulli beam theory can be used to calculate their deflection behavior.
- The dimension b of the flexures in the z-direction is large enough for the beams to be considered rigid in that direction in comparison with in-plane stiffness. We thus analyze the effect of loads in the xy-plane only.
- The restoring torque caused by the parasitic shift of the RCC flexures is negligible. Note that this is a standard assumption in the analysis of flexure pivots, see Refs. [35,38].
- The center of mass of the system is in point O as defined in Sec. 3 and stays there for any rotation. The effect of gravity is then equivalent to a force applied in point O.
- The parallel flexures do not transmit any force along their sliding axis. This assumption is reasonable knowing that their stiffness is much smaller than that of the "blocked" degrees-of-freedom of the flexure joints. It is assumed that the possible stiffening of the parallel flexures caused by gravity [13] is not sufficient to invalidate this assumption.

5.1 Rotational Stiffness of the Remote Center of Compliance Pivot Subject to Gravity. We use Euler-Bernoulli beam theory to compute the stiffness of an RCC pivot subject to gravity, considering each flexure as a cantilever beam under axial loading with a rotation θ prescribed at its extremity. The axial forces in the beams due to an external load F applied on the mobile part in point O at an angle φ such as depicted in Fig. 17 are

$$P_1 = \frac{F}{2}\left(\frac{\sin\varphi}{\sin\alpha} + \frac{\cos\varphi}{\cos\alpha}\right) \tag{25}$$

and

$$P_2 = \frac{F}{2}\left(-\frac{\sin\varphi}{\sin\alpha} + \frac{\cos\varphi}{\cos\alpha}\right) \tag{26}$$

Following the derivation of Eqs. (1)–(7) in Ref. [18] with these two axial loads, the stiffness of the loaded RCC becomes

$$k_R = k_{R,0} + \frac{EI_R}{12600L_R}\left[1680\bar{F}(9\delta^2+9\delta+1)\frac{\cos\varphi}{\cos\alpha} - \bar{F}^2(9\delta^2+9\delta+11)\frac{\cos^2\varphi}{\cos^2\alpha} + \bar{F}^2(9\delta^2+9\delta+11)\frac{\sin^2\varphi}{\sin^2\alpha}\right] + \mathcal{O}(\theta^2) + \mathcal{O}(\bar{F}^3) \tag{27}$$

The stiffness is expressed using series expansions at $F=0$ for small loads and $\theta=0$ for small amplitudes, where $k_{R,0}$ is the nominal stiffness of the RCC for an infinitesimal rotation in absence of external load given in Eq. (18) and

$$\bar{F} = \frac{FL_R^2}{EI_R} \tag{28}$$

is the normalized external load on the pivot.

5.2 Rotational Stiffness of the Half Co-RCC Subject to Gravity. The slider placed between the RCC and the body on which the gravity load is applied allows only for forces along u to be transmitted to the RCC, see Sec. 3.3. The resulting rotational stiffness of the half co-RCC is obtained by substituting $\varphi = 90$ deg in Eq. (27), giving

$$k_h(\bar{F}) = k_{R,0} - \frac{EI_R}{L_R}\frac{9\delta^2+9\delta+11}{12600\sin^2\alpha}\bar{F}^2 + \mathcal{O}(\theta^2) + \mathcal{O}(\bar{F}^3) \tag{29}$$

Remark. We can see that with the co-RCC design, the deviation from the nominal stiffness due to the external load has gone from first order $\bar{F}$ in Eq. (27) to second-order $\bar{F}^2$, which is the effect desired for achieving gravity insensitivity, see Sec. 1.5.

5.3 Rotational Stiffness of the Co-RCC Subject to Gravity. For a gravity load F acting on the co-RCC at an angle ψ with the x-axis, the RCC pivots 1 and 2 support the component of the load along their local u-axis, respectively, $F_1 = F\cos\psi$ and $F_2 = F\sin\psi$.

In order to calculate the effect of gravity on the co-RCC stiffness, we replace the nominal stiffness of the RCC pivots $2k_{R,0}$ in Eq. (17) with the stiffness of the loaded half co-RCC elements $k_h(\bar{F}_1) + k_h(\bar{F}_2)$, yielding

$$k_c(\bar{F}) = 2k_{R,0} - \frac{EI_R}{L_R}\frac{9\delta^2+9\delta+11}{12600\sin^2\alpha}\bar{F}^2(\sin^2\psi + \cos^2\psi) + \mathcal{O}(\theta^2) + \mathcal{O}(\bar{F}^3) = 2k_{R,0} - \frac{EI_R}{L_R}\frac{9\delta^2+9\delta+11}{12600\sin^2\alpha}\bar{F}^2 + \mathcal{O}(\theta^2) + \mathcal{O}(\bar{F}^3) \tag{30}$$

We now have an element whose only DOF is a rotation and whose stiffness is gravity-insensitive: the deviation from the nominal stiffness due to the external load is of second-order and the result is independent of the direction ψ of gravity. Note that this last property is obtained through the 90 deg angle between the two half co-RCC elements.

5.4 Gravity Sensitivity in Terms of Daily Rate. In horological terms, gravity sensitivity is specified by the daily rate caused by a change in the orientation of the oscillator with respect to gravity. From Eq. (7), one can express the gravity sensitivity of an oscillator with nominal stiffness k_0 and stiffness k under gravity load

$$\rho = 43200\frac{k-k_0}{k_0} + \mathcal{O}((k-k_0)^2) \tag{31}$$

This expression is obtained using Taylor series expansion around $k=k_0$ for a rotational oscillator with frequency $\omega = \sqrt{k/J}$, see Sec. 4.1.

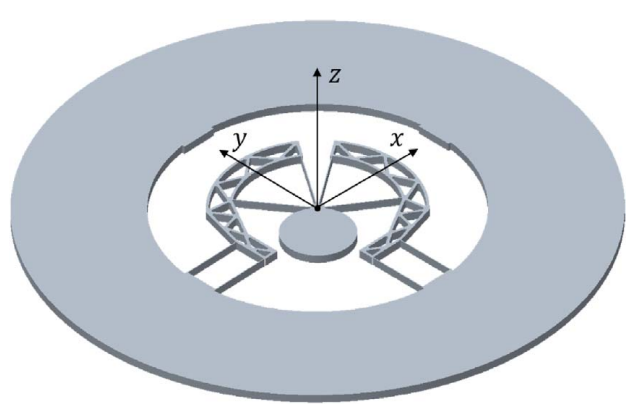

Fig. 18 Example embodiment of a co-RCC oscillator

Using Eq. (30) and neglecting the load effects of order >2 due to our small load assumption, the gravity sensitivity of the co-RCC is

$$\rho(\bar{F}) \approx 43200\frac{k_c(\bar{F}) - k_c(0)}{k_c(0)} \approx -\frac{3}{14}\frac{9\delta^2 + 9\delta + 11}{(3\delta^2 + 3\delta + 1)\sin^2\alpha}\bar{F}^2 \quad (32)$$

6 Dimensioning and Numerical Validation

We give here an example of dimensions for a co-RCC oscillator reaching the practical specifications listed in Sec. 6.1. The resulting geometry is depicted in Fig. 18. We use this oscillator for the numerical validation of the model using the finite element method (FEM).

6.1 Practical Watch Specifications. The following specifications are used as guidelines for our dimensioning

(1) Isochronism defect of order 1 s/day over the operating stroke.
(2) Daily rate stability in all orientations with respect to gravity within 5 s/day.
(3) Nominal amplitude of operation of 15 deg, assuming that this will be sufficient for an escapement to work.
(4) Amplitude variation of 10% during normal operation.
(5) Planar design compatible with standard microfabrication processes.

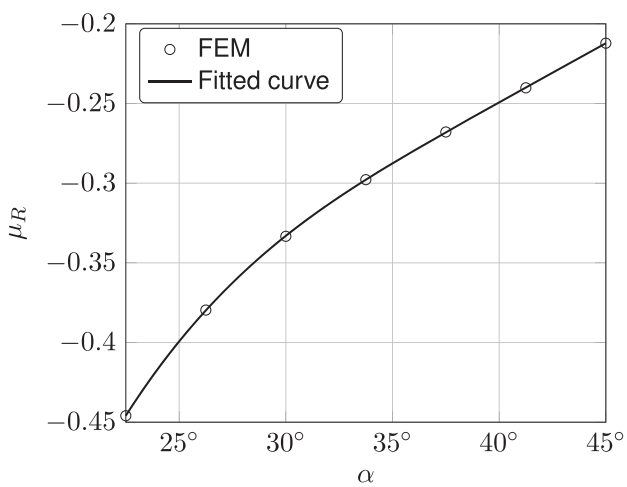

Fig. 19 Relative nonlinearity μ_R of the example RCC pivot versus α. The data are fitted with a Fourier model (with period π due to symmetry): $\mu_R(\alpha) = -2.6 + 0.14\cos 2\alpha + 3.1\sin 2\alpha + 0.76\cos 4\alpha - 0.17\sin 4\alpha$

6.2 Example of Dimensioning. The geometry of the co-RCC pivot can be described by the following set of dimensionless parameters for which we give the values chosen in this dimensioning:

- $\alpha = 34.7$ deg
- $\beta = b/h = 20$
- $\gamma = L_R/h = 347$
- $\delta = d/L_R = 0.1$
- $\lambda = 0.72$
- $\bar{F} = 0.92$

The geometry of the RCC flexures is illustrated in Fig. 17 and the parallel flexures are chosen to have the same cross-section ($I_p = I_R$). Note that the normalized load $\bar{F}$ results from the weight of the chosen inertial mass.

These dimensions correspond to a watch mechanism and are compatible with standard microfabrication processes such as DRIE. The crossing point δ is chosen so as to maximize the stroke of the pivot (in order to reach specifications 3 and 4 of Sec. 6.1) while keeping a feasible planar architecture satisfying specification 5 of Sec. 6.1. The maximum admissible stroke of a crossed flexure pivot is actually obtained when $\delta = -0.5$ (see Eq. 14 in Ref. [17]) but values smaller than $\delta = 0.1$ would bring the flexures too close to each other or need a design in two planes. The values of β and γ are chosen to allow for a large stroke while keeping sufficient out-of-plane stiffness. For materials with a ratio $\sigma_{\text{adm}}/E > 0.44\%$, such as silicon or some titanium alloys, the pivot only reaches the admissible bending stress σ_{adm} for strokes $\theta > 19$ deg, see Eq. (14) in Ref. [18], thus satisfying specification 3 and 4 of Sec. 6.1.

The values of α and λ were chosen to reach isochronism (see Sec. 6.2.1) and a constant gravity sensitivity of −5 s/day with the chosen normalized load $\bar{F}$. Any arbitrary value of gravity sensitivity could have been chosen as long as it stays constant, such as predicted by Eq. (32). However, we know that our analytical model is not perfect and chose a gravity sensitivity of −5 s/day assuming that any deviation would stay of the same order and thus satisfy specification 2 of Sec. 6.1.

6.2.1 Isochronism Tuning. We explained in Sec. 4.3 that the isochronism defect of the co-RCC could be tuned using the parameter λ, by varying the length L_p of the parallel flexures. Figure 6 displays the influence of λ on the isochronism of the example co-RCC. The numerical estimates for the isochronism defect are calculated in terms of the daily rate at $\Theta = 16.5$ deg with respect to reference amplitude $\Theta_1 = 15$ deg using Eq. (24). This corresponds to a 10% amplitude variation with respect to the reference amplitude in accordance with the specifications of Sec. 6.1.

Figure 6 shows that λ can be used to introduce a range of positive or negative isochronism defects up to the order ±100 s/day.

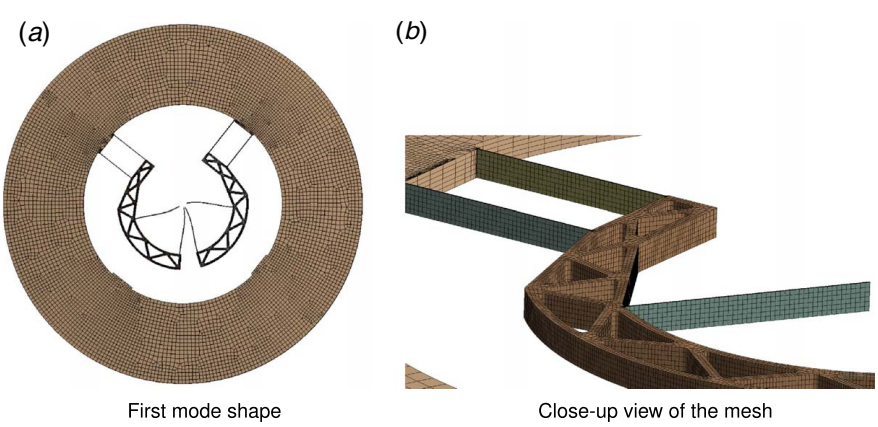

Fig. 20 Finite element model of the co-RCC oscillator: (*a*) first-mode shape and (*b*) close-up view of the mesh

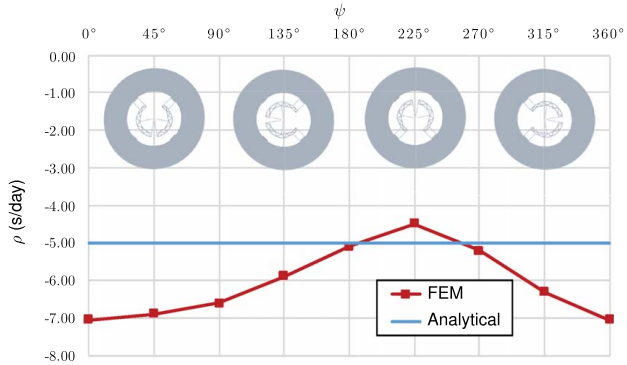

Fig. 21 Gravity sensitivity in s/day of the co-RCC oscillator versus the angle ψ of the gravity load in the *xy*-plane

This means that a value of λ can be found such that the oscillator is isochronous, i.e., $\rho = 0$, or that significant isochronism defects external to the oscillator can be compensated.

In order to satisfy specification 1 of Sec. 6.1, one has to estimate the step size $\Delta\lambda$ that corresponds to step size $\Delta\rho$ of 1 s/day. Given the dimensions specified in Sec. 6.2, the slope of the daily rate around the operating point ($\alpha = 34.7$ deg and $\lambda = 0.72$) is -560 s/day, see Fig. 6, which means that a rate variation of $\Delta\rho = 1$ s/day corresponds to a variation $\Delta\lambda/\lambda = 0.25\%$. For parallel flexures with a length L_p of order 1 mm, this corresponds to a change in length of order 2.5 μm, which is compatible with DRIE and laser ablation. Note that this resolution can be increased by setting the operating point where the slope of $\rho(\lambda)$ is smaller. For example, around the operating point $\lambda = 1$ in Fig. 6, $\Delta\rho = 1$ s/day is obtained with a 0.65% variation of λ.

Figure 6 also shows that for pivots with different values of RCC nonlinearity, characterized here by different values of α, a value of λ can be found such that the oscillator is isochronous. The influence of α on the relative nonlinearity μ_R of the RCC is shown in Fig. 19.

Remark. The parameter α affects both terms of the co-RCC nonlinearity in Eq. (20) and can be used as a design parameter to offset the isochronism tuning curve, see Fig. 6. As mentioned in Sec. 4.2.4, the RCC nonlinearity μ_R is calculated numerically using the method described in Sec. 6.3.1. In order to get an expression with respect to α, we fit a curve through a set of FEM-calculated data points depicted in Fig. 19.

6.3 Numerical Validation. We validate the analytical models described in Secs. 4 and 5 by simulating the example co-RCC depicted in Fig. 18 using the commercial FEM software ANSYS [44]. We use a mesh of hexahedral elements of type SOLID186 that is refined on the flexures such that there are three elements across their thickness h and six along their height b. The number of elements along the length of the flexures is chosen such that the elements have a square face. The meshing can be seen in Fig. 20. Since we are interested in the nonlinear behavior of our system, the structural analyses are performed with the large deflection setting.

6.3.1 Isochronism Validation. We evaluate the nonlinearity of a pivot by FEM from its torque-angle relationship. We apply 50 incremental displacement values from 0 to 10 deg on the mobile end of the pivot and measure the reaction torque on the fixed frame. We then fit an odd cubic polynomial to the torque-angle relationship and extract the relative nonlinearity using Eq. (20). This method is used to calculate the relative nonlinearity of the RCC for the analytical model, see Fig. 19, and to calculate the relative nonlinearity of the co-RCC for the numerical validation.

The analytical and numerical results are compared in terms of daily rate, from the relative restoring torque nonlinearity, using Eq. (8). The results are computed for different values of λ and α and plotted in Fig. 6, showing a good match that validates the analytical component of the model.

For the values of design parameters chosen to reach isochronism ($\alpha = 34.7$ deg and $\lambda = 0.72$), the simulation returns a restoring torque nonlinearity $\mu = -0.0024$ corresponding to a daily rate $\rho = -1.1$ s/day at $\Theta = 16.5$ deg with respect to reference amplitude $\Theta_1 = 15$ deg, thus satisfying specification 1 of Sec. 6.1. Note that the remaining defect could be the result of numerical errors or, if this is not the case, could be further reduced by fine-tuning the value of L_p.

6.3.2 Gravity Sensitivity Validation. We simulate the gravity sensitivity of the pivot by subjecting it to standard earth gravity and extracting the frequency of its first-vibration mode, see Fig. 20(*a*). In order to be consistent with the theoretical model, the masses of the intermediate bodies and flexures are set to zero and the center of mass is in point O. The data are collected for accelerations in the *xy*-plane with orientation ψ spanning the interval from 0 to 360 deg, and the daily rate with respect to operation without gravity calculated with Eq. (7) is displayed in Fig. 21.

The gravity sensitivity obtained by FEM simulation varies between -4.5 and -7 s/day whereas Eq. (32) returns a constant value of -5 s/day with the dimensions given in Sec. 6.2. Considering the order of magnitude observed (a 1 s/day rate variation corresponds to a 10 parts per million frequency variation), the results are close enough to validate the model.

The numerical solution shows a daily rate of -5.75 ± 1.25 s/day which is well within the practical mechanical watch specification 2 of Sec. 6.1. Note that the constant offset of -5.75 s/day is not problematic since it can be compensated by tuning the nominal frequency of the oscillator. This can be done by varying its inertia and is a standard procedure for watchmakers.

Remark. The differences between the analytical model and the numerical solution could be explained by a shift of the center of mass of the pivot due to the u-component of the RCC parasitic shift that is neglected in our model, see Sec. 3.2.1. This assumption is coherent with the symmetric maximum and minimum observed at 45 and 225 deg, corresponding to the axis of symmetry of the architecture.

7 Conclusion

This article presents a new way of tuning the isochronism of flexure-based mechanical time bases by taking advantage of their parasitic motion. We highlighted the importance of isochronism in the development of precision mechanical time bases and situated our contribution in this context. We invented a new flexure pivot we called the co-RCC that integrates the new isochronism tuning method in a gravity-insensitive architecture. We provided an analytical model that can be used to dimension an oscillator and validated it by numerical simulation. We showed that the concept can be embodied in a compact architecture that is compatible with microfabrication. Our future work will consist in the experimental validation of the co-RCC concept and the exploration of new ways to tune the isochronism of flexure-based mechanical oscillators.

Acknowledgment

The authors would like to thank Simón Prêcheur-Llarena for fabricating the mock-up of Fig. 5.

References

[1] Académie des inscriptions et belles-lettres, 1675, *Le Journal Des Sçavans*, Jean Cusson, Paris, France.
[2] Bateman, D. A., 1977, "Vibration Theory and Clocks," Horological J., **120–121**(1), pp. 3–8.
[3] Matthys, R. J., 2004, *Accurate Clock Pendulums*, Oxford University Press, Oxford.

[4] Vardi, I., 2014, "Le facteur de qualité en horlogerie mécanique," Bulletin de la Société Suisse de Chronométrie, **75**, pp. 9.
[5] Eastman, F. S., 1935, *Flexure Pivots to Replace Knife Edges and Ball Bearings, An Adaptation of Beam-Column Analysis* (Engineering Experiment Station Series, University of Washington), Seattle, WA.
[6] Noell, W., Clerc, P.-A., Jeanneret, S., Hoogerwerf, A., Niedermann, P., Perret, A., and de Rooij, N., 2004, "MEMS for a Watches," Maastricht MEMS 2004 Technical Digest, IEEE, Maastricht, Netherlands, p. 39904.
[7] Musy, J.-P., Maier, F., and Krüttli, A., 2008, "Echappement et spiral réalisés en Silinvar®," Journée d'Etude de la Société Suisse de Chronométrie, La Chaux-de-Fonds, pp. 51–54.
[8] Barrot, F., Dubochet, O., Henein, S., Genequand, P., Giriens, L., Kjelberg, I., Renevey, P., Schwab, P., and Ganny, F., 2014, "Un nouveau régulateur mécanique pour une réserve de marche exceptionnelle," Actes de La Journée d'Etude de La Société Suisse de Chronométrie, pp. 43–48.
[9] Roulet, C., 2017, "Zenith's Quantum Leap," journal.hautehorlogerie.org/en/zeniths-quantum-leap/
[10] Semon, G., Ypma, W. J. B., Weeke, S. L., and Tolou, N., 2017, "Device for a Timepiece, Timepiece Movement and Timepiece Comprising a Device of Said Type," worldwide.espacenet.com/publicationDetails/biblio?FT=D&date=20170921&DB=&locale=&CC=WO&NR=2017157870A1&KC=A1&ND=1
[11] von Gunten, S., Gygax, P., and Humair, L., 2015, "Oscillateur Mécanique," U.S. Patent EP2273323B1.
[12] Markl, X., 2019, "Introducing Ulysse Nardin Freak NeXt," monochrome-watches.com/ulysse-nardin-freak-next-a-new-concept-with-revolutionary-3d-flying-oscillator-live-pics/
[13] Cosandier, F., Henein, S., Richard, M., and Rubbert, L., 2017, *The Art of Flexure Mechanism Design*, EPFL Press, Lausanne, Switzerland.
[14] Howell, L. L., 2001, *Compliant Mechanisms*, Wiley, New York.
[15] Matthews, M. R., 1994, *Science Teaching: The Role of History and Philosophy of Science*, Routledge, New York.
[16] Huygens, C., "Horologium Oscillatorium [Latin with English translation by Ian Bruce]," www.17centurymaths.com/contents/huygenscontents.html
[17] Weeke, S. L., Tolou, N., Semon, G., and Herder, J. L., 2016, "A Fully Compliant Force Balanced Oscillator," ASME 2016 International Design Engineering Technical Conferences and Computers and Information in Engineering Conference. Volume 5A: 40th Mechanisms and Robotics Conference, Charlotte, NC, Aug. 21–24, American Society of Mechanical Engineers, p. V05AT07A008.
[18] Kahrobaiyan, M. H., Thalmann, E., Rubbert, L., Vardi, I., and Henein, S., 2018, "Gravity-Insensitive Flexure Pivot Oscillators," ASME J. Mech. Des., **140**(7), p. 075002.
[19] Conus, T., 2015, "Swatch Sistem51", Journée d'Etude de La Société Suisse de Chronométrie 2015, pp. 105–111.
[20] Guillaume, C.-E., 1920, "Nobel Lecture: Invar and Elinvar," old.nobelprize.org/nobel_prizes/physics/laureates/1920/guillaume-lecture.html
[21] Ching, H., and Ko, P. H., 2016, "Silicon Hairspring," U.S. Patent No. US20160238994A1.
[22] Vardi, I., 2015, "Mathematics, the Language of Watchmaking," Watch Around, **20**, pp. 90–94.
[23] Bernoulli, J., 1697, "Curvatura radii in diaphanis non uniformibus, Solutioque Problematis a se in Actis 1696, p. 269, propositi, de invenienda Linea Brachystochrona, id est, in qua grave a dato puncto ad datum punctum brevissimo tempore decurrit, & de curva Synchrona seu radiorum unda construenda," *Acta Eruditorum*, Vol. 19, Prostant apud J. Grossium and J. F. Gleditschium, eds., pp. 206–211.
[24] Beckett, E., and Grimthorpe, L., 1903, *A Rudimentary Treatise on Clocks, Watches and Bells*, 8th ed., Crosby Lockwood and Son, D. Van Nostrand Company, London.
[25] Rawlings, A. L., 1993, *The Science of Clocks & Watches*, 3rd revised ed., British Horological Institute, Upton, UK,
[26] Fedchenko, F. M., 1957, "Astronomical Clock AChF-1 With Isochronous Pendulum," Sov. Astron., **1**, p. 637.
[27] Huygens, C., 1893, *Oeuvres Complètes*, Publiées par la société hollandaise des sciences ed., Vol. VII. Martinus Nijhoff, La Haye.
[28] Hastings, P., 1993, "A Look At the Grasshopper Escapement," Horological J., **136**(2), pp. 48–53.
[29] Wittrick, W., 1948, "The Theory of Symmetrical Crossed Flexure Pivots," Aust. J. Sci. Res. A: Phys. Sci., **1**(2), p. 121.
[30] Henein, S., and Kjelberg, I., 2015, "Timepiece Oscillator," U.S. Patent No. US9207641.
[31] Wittrick, W., 1951, "The Properties of Crossed Flexure Pivots, and the Influence of the Point at Which the Strips Cross," Aeronaut. Q., **2**(4), pp. 272–292.
[32] Henein, S., and Schwab, P., 2014, Isochronism Corrector for Clockwork Escapement and Escapement Provided With Such a Corrector," U.S. Patent No. US8672536B2.
[33] Woodward, P., 1995, *My Own Right Time: An Exploration of Clockwork Design*, Oxford University Press, Oxford.
[34] Di Domenico, G., Hinaux, B., Klinger, L., and Helfer, J.-L., 2016, Timepiece Resonator With Crossed Blades," worldwide.espacenet.com/publicationDetails/biblio?FT=D&date=20160623&DB=EPODOC&locale=en_EP&CC=WO&NR=2016096677A1&KC=A1&ND=4
[35] Zhao, H., and Bi, S., 2010, "Accuracy Characteristics of the Generalized Cross-Spring Pivot," Mech. Mach. Theory, **45**(10), pp. 1434–1448.
[36] Pei, X., Yu, J., Zong, G., Bi, S., and Yu, Z., 2008, "Analysis of Rotational Precision for An Isosceles-Trapezoidal Flexural Pivot," ASME J. Mech. Des., **130**(5), p. 052302.
[37] Di Domenico, G., Léchot, D., Helfer, J.-L., and Winkler, P., 2017, "Timepiece Resonator Mechanism," worldwide.espacenet.com/publicationDetails/biblio?FT=D&date=20170816&DB=&locale=en_EP&CC=EP&NR=3206089A1&KC=A1&ND=4
[38] Zhao, H., and Bi, S., 2010, "Stiffness and Stress Characteristics of the Generalized Cross-Spring Pivot," Mech. Mach. Theory, **45**(3), pp. 378–391.
[39] Haringx, J. A., 1949, "The Cross-Spring Pivot as a Constructional Element," Flow, Turbul. Combust., **1**(1), p. 313.
[40] Grübler, M., 1917, *Getriebelehre: Eine Theorie Des Zwanglaufes Und Der Ebenen Mechanismen*, Springer-Verlag, Berlin Heidelberg.
[41] Thalmann, E., Kahrobaiyan, M. H., and Henein, S., 2018, "Flexure-Pivot Oscillator Restoring Torque Nonlinearity and Isochronism Defect," ASME 2018 International Design Engineering Technical Conferences and Computers and Information in Engineering Conference. Volume 5A: 42nd Mechanisms and Robotics Conference, Quebec City, Quebec, Canada, Aug. 26–29, American Society of Mechanical Engineers, New York, p. V05AT07A013.
[42] Reymondin, C.-A., Monnier, G., Jeanneret, D., and Pelaratti, U., 1999, *The Theory of Horology*, Swiss Federation of Technical Colleges, Le Locle, Switzerland.
[43] Vardi, I., Rubbert, L., Bitterli, R., Ferrier, N., Kahrobaiyan, M., Nussbaumer, B., and Henein, S., 2018, "Theory and Design of Spherical Oscillator Mechanisms," Precis. Eng., **51**, pp. 499–513.
[44] ANSYS® Academic Research Mechanical, Release 19.2, Help System, Theory Reference, ANSYS Inc.